ACS Catalysis

Research Article

Cite This: ACS Catal. 2018, 8, 10658−10667

pubs.acs.org/acscatalysis

Tuning Reactivity of Bioinspired [NiFe]-Hydrogenase Models by Ligand Design and Modeling the CO Inhibition Process

Deborah Brazzolotto,[†,‡,#] Lianke Wang,[†,#] Hao Tang,[§,#] Marcello Gennari,[†] Nicolas Queyriaux,[‡] Christian Philouze,[†] Serhiy Demeshko,[∥] Franc Meyer,[∥] Maylis Orio,[⊥] Vincent Artero,[*,‡] Michael B. Hall,[*,§] and Carole Duboc[*,†]

[†]Université Grenoble Alpes, UMR CNRS 5250, Département de Chimie Moléculaire, F-38000 Grenoble, France

[‡]Université Grenoble Alpes, UMR CNRS 5249, CEA, Laboratoire de Chimie et Biologie des Métaux, F-38000 Grenoble, France

[§]Department of Chemistry, Texas A&M University, College Station, Texas 77845, United States

[∥]University of Göttingen, Insitute für Anorganische Chemie, Tammannstrasse 4, D- 37077 Göttingen, Germany

[⊥]Institut des Sciences Moléculaires de Marseille, Aix Marseille Université, CNRS, Centrale Marseille, ISM2 UMR 7313, 13397 Marseille, France

Supporting Information

ABSTRACT: Despite the report of several structural and functional models of the [NiFe]-hydrogenases, it is still unclear how the succession of electron and proton transfers during H_2 production catalysis are controlled in terms of both sequence (order of the chemical or redox steps) and sites (metal and/or ligand). To address this issue, the structure of the previously described bioinspired [NiFe]-hydrogenase complex $[L^{N2S2}Ni^{II}Fe^{II}Cp(CO)]^+$ (**$LNi^{II}Fe^{II}Cp$**, with L^{N2S2} = 2,2′-(2,2′-bipyridine-6,6′-diyl)bis(1,1′-diphenylethanethiolate) and Cp = cyclopentadienyl) has been fine-tuned by modifying exclusively the Fe site. In $[L^{N2S2}Ni^{II}Fe^{II}Cp^*(CO)]^+$ (**$LNi^{II}Fe^{II}Cp^*$**, with Cp* = pentamethylcyclopentadienyl), the Cp^- ligand has been replaced by Cp^{*-} to change both the redox and structural properties of the overall complex as a consequence of the steric hindrance of Cp^{*-}. The **$LNi^{II}Fe^{II}Cp^*$** complex acts as an efficient electrocatalyst to produce H_2. Density functional theory (DFT) calculations support a CEEC cycle, following an initial reduction. The initial protonation leads to the cleavage of one thiolate−iron bond and the next reduction to the generation of a bridging Fe-based hydride moiety. Interestingly, the second protonation step generates a species containing a terminal Ni-based thiol and a bridging hydride. In the presence of CO, the electrocatalytic activity of **$LNi^{II}Fe^{II}Cp^*$** for H_2 production is markedly inhibited (about 90% of loss), while only a partial inhibition (about 30% of loss) is observed in the case of **$LNi^{II}Fe^{II}Cp$**. DFT calculations rationalized this effect by predicting that interactions of the one- and two-electron-reduced species for **$LNi^{II}Fe^{II}Cp^*$** with CO are thermodynamically more favorable in comparison to those for **$LNi^{II}Fe^{II}Cp$**.

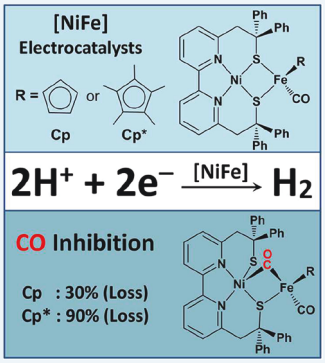

KEYWORDS: *bioinspired chemistry, hydrogenases, electrocatalysis, small-molecule activation, H_2 production, nickel, iron*

Downloaded via TEXAS A&M UNIV COLG STATION on April 11, 2019 at 22:21:54 (UTC).
See https://pubs.acs.org/sharingguidelines for options on how to legitimately share published articles.

INTRODUCTION

[NiFe]-hydrogenases catalyze the reversible reduction of protons into dihydrogen and function at ambient temperature and pressure with a low overpotential requirement.[1,2] The active site of [NiFe]-hydrogenases is composed of a unique heterodinuclear NiFe complex, in which the two metal sites are bridged by two thiolates from cysteine residues (Scheme 1).[3] The coordination sphere of nickel is completed by two terminal cysteinates and that of iron by two CN^- and one CO ligands. In the currently proposed catalytic mechanism, the two electrons and two protons required to form H_2 are supplied to the active site in a controlled and sequential four-step pathway.[1,4−6] The $Ni^{II}Fe^{II}$ initial state (*Ni-SI$_a$*) is first reduced to a $Ni^{I}Fe^{II}$ intermediate (*Ni-L*),[7−10] which is successively protonated to generate a first $Ni^{III}(\mu\text{-H})Fe^{II}$ hydride species (*Ni-C*).[11,12] *Ni-C* is then reduced by one electron and protonated to produce the corresponding $(SH)Ni^{II}(\mu\text{-H})Fe^{II}$ species (*Ni-R*),[13,14] which promptly releases H_2 and regenerates *Ni-SI$_a$*. This nickel-centered mechanism thus follows an ECEC pathway (E = electron transfer, C = chemical reaction, here corresponding to a proton transfer). Hydrogenase activity has been shown to be inhibited in the presence of carbon monoxide.[15−17] Two CO-binding states, *Ni-SCO* (Ni^{II}−CO)[18,19] and *Ni-CO* (Ni^{I}−CO)[15,19] are generated by direct reaction of CO with the *Ni-SI$_a$* and *Ni-L* states, respectively (Scheme 1) and have been thoroughly characterized. *Ni-SCO* is the sole CO adduct that is currently proposed to be involved in the CO inhibition process,[7,9,10] but the recent implication of *Ni-L* as a catalytic intermediate in the H^+/H_2 interconversion mechanism calls for further investigation.

Received: July 18, 2018
Revised: September 27, 2018
Published: October 4, 2018

© 2018 American Chemical Society

DOI: 10.1021/acscatal.8b02830
ACS Catal. 2018, 8, 10658−10667

Scheme 1. Proposed Catalytic Cycle of the [NiFe]-Hydrogenase and Inhibition Process in the Presence of CO[a]

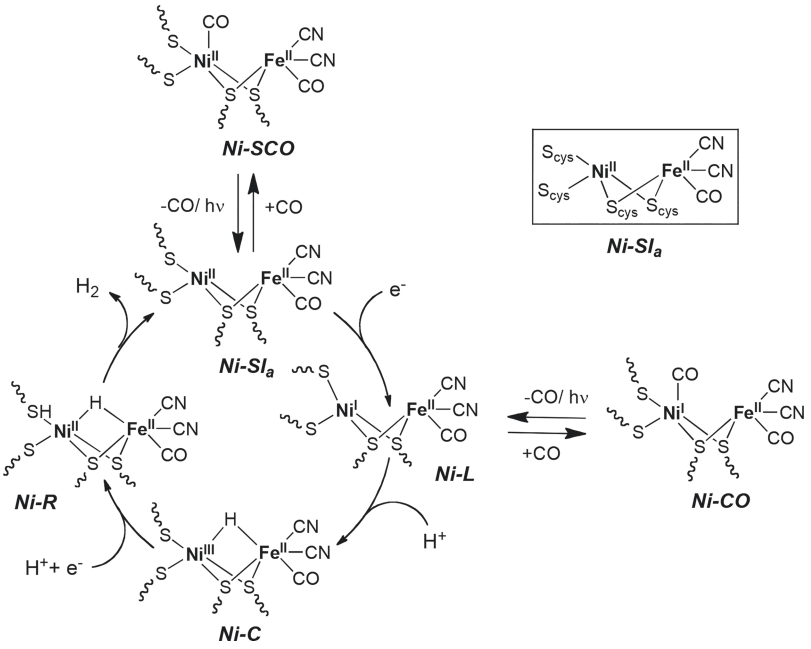

[a]The inset gives a schematic representation of the active site in the *Ni-SI*$_a$ state.

Scheme 2. Synthesis of [LNi^{II}Fe^{II}Cp$^{(*)}$]BF$_4$

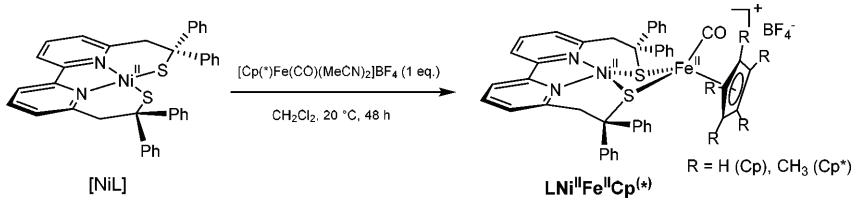

Modeling the singular structure and unrivaled reactivity of the [NiFe]-hydrogenases is critical not only to gain a deeper understanding of the enzymatic mechanism but also to develop economically and environmentally viable catalysts for H_2 production.[20−23] Among the existing bioinspired NiFe complexes, few display reactivity localized, at least partially, at the Ni site,[24−26] while in most cases the H^+ reduction process and the generation of hydride species occur on the Fe site. McMaster and Schröder reported the first *Ni-L* model, but this species proved inactive toward proton reduction.[25] Rauchfuss and Lubitz demonstrated that the first reduction process of a NiFe H_2-evolving electrocatalyst is centered on nickel,[24] even though protonation of the generated Ni^IFe^{II} intermediate affords a hydride terminally bound to iron, as suggested by DFT calculations.

Several bioinspired NiFe complexes[27,28] have also been described in the past decade using a $(L^{N2S2/S4})Ni^{II}$ unit combined with $[CpFe^{II}(CO)(MeCN)_2]^+$ and display moderate activity.[28] More recently, we have described a bioinspired NiFe complex, $[L^{N2S2}Ni^{II}Fe^{II}Cp(CO)]^+$ (with L^{N2S2}= 2,2′-(2,2′-bipyridine-6,6′-diyl)bis(1,1′-diphenylethanethiolate); **LNi^{II}Fe^{II}Cp** in Scheme 2), that reproduces the structural features and function of the active site of [NiFe]-hydrogenase with redox chemistry mainly centered on the Ni site. We were also able to isolate and experimentally characterize an active Ni^IFe^{II} intermediate modeling the *Ni-L* state and to generate a $Ni^{II}Fe^{II}$ hydride species.[26] A mechanistic theoretical investigation carried out by Hall et al.[29] revealed that the hydride ligand is actually bridging the two metallic ions (instead of terminally Ni bound as suggested in the initial study),[26] which is made possible thanks to the hemilability of the bridging dithiolate L^{N2S2} ligand.[30] Such a hemilability property was previously observed for other dithiolato-bridged Ni−Fe complexes, including one with a {Fe(CO)Cp} unit reported by Darensbourg and Hall.[31−34] However, the $Ni^{II}Fe^{II}$ hydride generated from **LNi^{II}Fe^{II}Cp** requires further reductive activation before H_2 evolution can proceed.[29]

The aim of the present work is to investigate the role of the Fe unit in the sequential electron and proton transfers during catalysis and the involved protonation/reduction sites: i.e. Fe, Ni, or ligand. For this purpose, we have modified the former **LNi^{II}Fe^{II}Cp** complex at the Fe site, keeping the Ni site unchanged. Specifically, we have replaced the Fe-bound cyclopentadienyl (Cp^-) by pentamethylcyclopentadienyl (Cp^{*-}) and studied how this modification affects the structural, redox, and electrocatalytic properties of the heterodinuclear complex. We also report here the effect of CO addition on the redox and catalytic activity of both the Cp^- and Cp^{*-} derivatives. Studies of the CO inhibition process on NiFe models only include two *Ni-SCO* models.[35,36] One reversibly binds CO at the Ni^{II} center, but no reactivity toward H^+ was reported.[36] The other displays H_2 evolution electrocatalytic activity, which is inhibited in the presence of CO, but CO binds to iron.[35,37]

DOI: 10.1021/acscatal.8b02830
ACS Catal. 2018, 8, 10658−10667

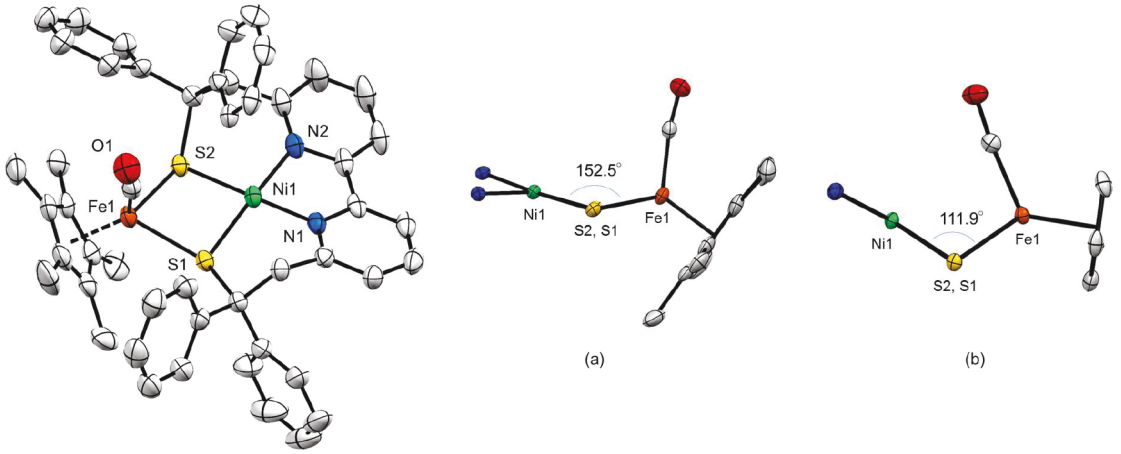

Figure 1. ORTEP view of the **LNi^{II}Fe^{II}Cp*** cation of $[LNi^{II}Fe^{II}Cp^*(CO)]BF_4 \cdot 0.69CH_2Cl_2 \cdot 0.15Et_2O \cdot 0.15H_2O$ (50% thermal ellipsoids, Ni···Fe = 3.391(6) Å, (SNiS)(SFeS) = 152.54 (4)°) and representations of the hinge angles found in the $\{NiFeS_2\}$ cores of (a) **LNi^{II}Fe^{II}Cp*** and (b) **LNi^{II}Fe^{II}Cp**.

RESULTS

Synthesis and Characterization of LNi^{II}Fe^{II}Cp*. The synthetic procedure previously used to isolate **LNi^{II}Fe^{II}Cp**[26] has been adapted for the synthesis and isolation of the corresponding Cp* derivative, $[L^{N2S2}Ni^{II}Fe^{II}Cp^*(CO)]^+$ (**LNi^{II}Fe^{II}Cp***), using $[Cp^*Fe^{II}(CO)(MeCN)_2]^+$ as the Fe precursor (see Scheme 2). The X-ray structure of the **LNi^{II}Fe^{II}Cp*** complex reveals a $\{NiFeS_2\}$ core with two bridging thiolate ligands similar to that of **LNi^{II}Fe^{II}Cp** (Figure 1 and Tables S1 and S2) but with significant geometric variations. In **LNi^{II}Fe^{II}Cp*** the Ni···Fe distance of 3.391 Å is significantly longer than in **LNi^{II}Fe^{II}Cp** (2.88(4) Å) or in the active site of [NiFe]-hydrogenases (~2.8 Å range),[38] leading to the quasi-planar $\{NiFeS_2\}$ diamond core. The hinge angle, defined by the intersection of the NiS_2 and FeS_2 planes, is 152.5°, and the $NiFeS_2$ atoms deviate less than 0.18 Å from the mean plane. For comparison, hinge angles of 107.2 and 111.9° and deviations from the $NiFeS_2$ mean plane up to 0.53−0.57 Å are found for the two crystallographically independent units of **LNi^{II}Fe^{II}Cp** with a butterfly structure (Figure 1). This most likely results from steric repulsion between the methyl substituents of Cp^{*-} and the phenyl rings of the L^{N2S2} ligand (see below). Apart from these differences, the same steroisomeric form is found in both Cp and Cp* derivatives with an exo conformation (Scheme S1).[39]

Fully optimized DFT calculations confirmed that for **LNi^{II}Fe^{II}Cp*** the quasi-diamond geometry of $\{NiFeS_2\}$ is more stable than the butterfly geometry by 3.3 kcal mol^{-1}, while that for **LNi^{II}Fe^{II}Cp** is less stable by 1.8 kcal mol^{-1}. The butterfly geometry has both six-membered rings (Ni−N−C−CH_2−CPh_2−S−) in boat conformations with respect to the Ni. These two boat conformations orient the S lone pairs[33] and shorten the Ni···Fe distance in the Cp complex, while in the Cp* complex such geometry is prevented because of the interactions between the phenyl and methyl groups. In **LNi^{II}Fe^{II}Cp***, it has been experimentally observed that the Ni site displays a distorted-square-planar geometry featuring a pseudotetrahedral twist angle (S−Ni−S/N−Ni−N) of 13.84°, notably smaller than in the mononuclear $[NiL^{N2S2}]$ precursor (29.15°)[40] but much larger than in **LNi^{II}Fe^{II}Cp** (5.47°). It is the inversion of one of the thiolate arms (N···S linker) in **LNi^{II}Fe^{II}Cp*** with respect to **LNi^{II}Fe^{II}Cp** that leads to the changes in the quasi-diamond (boat−chair) vs butterfly (boat−boat) geometries and the twist angles. This demonstrates the geometrical flexibility of the Ni site surrounded by the L^{N2S2} ligand.

The ESI-mass spectrum of a MeCN solution of **LNi^{II}Fe^{II}Cp*** displays a peak at m/z 855.2, corresponding to $[L^{N2S2}Ni^{II}Fe^{II}Cp^*(CO)]^+$ (Figure S1), indicating that its dinuclear structure is preserved in solution. As in the case of **LNi^{II}Fe^{II}Cp**, the Ni^{II} and Fe^{II} ions are low spin (S = 0), resulting in a diamagnetic complex, as attested by EPR silence and diamagnetic ^{1}H NMR spectra in MeCN (Figure S2). The low-spin state of the Fe^{II} ion is confirmed by its Mössbauer spectrum (Figure S3), which displays a doublet with isomer shift (δ = 0.44 mm s^{-1}) and quadrupole splitting (ΔE_Q = 1.79 mm s^{-1}) values that are close to those found for **LNi^{II}Fe^{II}Cp** (δ = 0.39 mm s^{-1} and ΔE_Q = 1.82 mm s^{-1}). Accordingly, the CO stretching vibration ($\bar{\nu}_{CO}$ 1926 cm^{-1}) is in the same range as for **LNi^{II}Fe^{II}Cp** ($\bar{\nu}_{CO}$ 1929 cm^{-1}), consistent with a similar environment of the Fe^{II} ion in both complexes. The selective NOE ^{1}H NMR spectrum (Figure S4) confirms the proximity between the CH_3 substituents of Cp* and phenyl rings of the L^{N2S2} ligand in MeCN solution, which forces the system to adapt a constrained quasi-planar $\{NiFeS_2\}$ core.

Redox and Electrocatalytic Properties of LNi^{II}Fe^{II}Cp*. The cyclic voltammogram (CV) of **LNi^{II}Fe^{II}Cp*** recorded in MeCN displays two one-electron-reduction processes and differs from that of **LNi^{II}Fe^{II}Cp**, for which the two reduction systems are reversible (Figure 2). The first apparently irreversible reduction of **LNi^{II}Fe^{II}Cp*** (E_{pc} = −1.46 V vs Fc^+/Fc) is associated with an oxidation peak at E_{pa} = −1.04 V. Upon an increase in the scan rate, the process becomes partially reversible (see Figure S5). It thus can be interpreted as a one-electron reduction that is followed by a rapid chemical reaction. By comparison with the CV of $[Cp^*Fe^{II}(CO)(MeCN)_2]^+$ recorded under the same conditions (Figure S6), we could assign the oxidation process at E_{pa} = −1.04 V to the oxidation of the reduced form of the mononuclear $[Cp^*Fe^{II}(CO)(MeCN)_2]^+$ fragment. We propose that the one-electron reduction of **LNi^{II}Fe^{II}Cp*** occurs at the Ni site as for **LNi^{II}Fe^{II}Cp** to generate $[L^{N2S2}Ni^{I}Fe^{II}Cp^*(CO)]$ (**LNi^{I}Fe^{II}Cp***) (see DFT Mechanistic Investigations).[26,29] **LNi^{I}Fe^{II}Cp*** is unstable on the CV time scale and undergoes decomposition into $[Ni^{II}L^{N2S2}]$ and the product of reduction of $[Fe^{II}Cp^*(CO)(MeCN)_2]^+$, defined as

DOI: 10.1021/acscatal.8b02830
ACS Catal. 2018, 8, 10658−10667

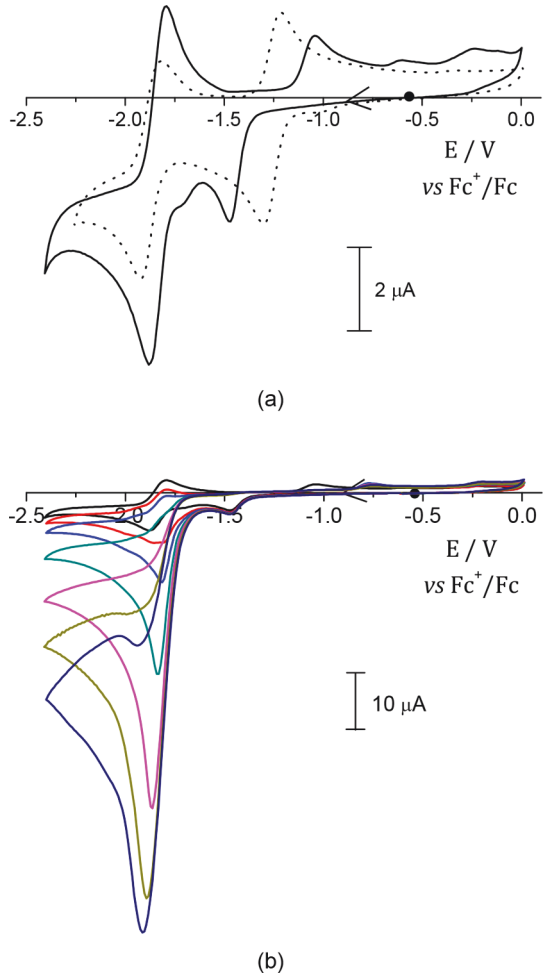

Figure 2. (a) CVs of 0.2 mM solutions of **LNi^{II}Fe^{II}Cp*** (solid line) and **LNi^{II}Fe^{II}Cp** (dotted line) in MeCN/0.1 M n-Bu_4NClO_4 recorded on a glassy-carbon working electrode at 100 mV s^{-1}. (b) CVs of the same **LNi^{II}Fe^{II}Cp*** solution before (black line) and after the addition of various amounts of $[Et_3NH]^+$: (red line) 1 equiv, (blue line) 2 equiv, (green line) 5 equiv, (pink line) 10 equiv, (olive line) 15 equiv, and (navy line) 20 equiv (same conditions as in (a)).

$[Cp^*Fe^I(CO)(MeCN)]$ by DFT calculations (see DFT Mechanistic Investigations). Consistently, the second reduction process displays a reversible signal at $E_{1/2}$ = −1.83 V (ΔE_p = 60 mV), which matches the cathodic signal of the mononuclear $[NiL^{N2S2}]$ complex corresponding to a bipyridine-centered one-electron-reduction process.[40] From variable scan rate experiments (see the Supporting Information), a first-order rate constant (k_{diss}) of 16(2) s^{-1} has been determined for the decomposition of **LNi^{I}Fe^{II}Cp*** into $[NiL^{N2S2}]$ and $[Cp^*Fe(CO)(MeCN)]$ (half-life time of **LNi^{I}Fe^{II}Cp*** ∼0.04 s; in the CV at 100 mV s^{-1}, the time between the two reduction systems, separated by about 300 mV, is ∼3 s). Dissociation is likely induced by the steric hindrance of both Cp^{*-} and L^{N2S2} ligands that precludes the CO ligand from bridging the two metallic ions, as confirmed by its DFT optimized structures. In contrast, it has been proposed that the bridging CO ligand stabilizes the **LNi^{I}Fe^{II}Cp** species.[29]

A 140 mV cathodic shift of the first Ni-centered reduction process is observed for **LNi^{II}Fe^{II}Cp*** with respect to **LNi^{II}Fe^{II}Cp** (E_{pc} = −1.32 V). This behavior can be due to (i) the more electron donating character of Cp^{*-} in comparison to Cp^-, leading to a larger electron density on thiolate ligands and, thus, indirectly on the Ni site in **LNi^{II}Fe^{II}Cp*** and/or to (ii) the difference in the $\{NiFeS_2\}$ core geometry (butterfly vs quasi-planar) that leads to structural changes around the redox-active Ni center, especially to different orientations of thiolate lone pairs with respect to the Ni atom. The discrepancy between the redox properties of **LNi^{II}Fe^{II}Cp** and **LNi^{II}Fe^{II}Cp*** illustrates how the organometallic iron unit (via either the electronic or steric properties of the Cp-type ligand) can modulate the electronics of the nickel center, as proposed in the case of [NiFe]-hydrogenase.[26]

The CV of **LNi^{II}Fe^{II}Cp*** is notably modified in the presence of 1−20 equiv of Et_3NHBF_4 (pK_a = 18.6 in MeCN,[41] Figure 2 and Figure S8). It can be observed that the signal at E_{pa} = −1.04 V present on the reverse scan of the CV of **LNi^{II}Fe^{II}Cp*** disappears, suggesting that dissociation of **LNi^{I}Fe^{II}Cp*** is prevented in the presence of protons.[42] In the presence of Et_3NHBF_4, a catalytic process ($E_{cat/2}$ = −1.86 V vs Fc^+/Fc, measured at the half-wave) develops on top of the second wave of **LNi^{II}Fe^{II}Cp***. The potential of this reversible redox system is similar to that of the $[NiL^{N2S2}]/[NiL^{N2S2}]^-$ couple, likely because both are centered at the bipyridine unit and are only slightly influenced by remote modifications. However, the shape of the H^+ reduction wave catalyzed by **LNi^{II}Fe^{II}Cp*** strongly differs from the corresponding waves observed in the presence of the two mononuclear $[NiL^{N2S2}]$ or $[Cp^*Fe^{II}(CO)(MeCN)_2]^+$ complexes (Figure S9).

Bulk electrolysis experiments performed at −1.85 V vs Fc^+/Fc on a Hg-pool cathode confirmed electrocatalytic production of H_2 in the presence of **LNi^{II}Fe^{II}Cp*** (Figure S10). The H_2 evolution performances (17 turnovers achieved with 76% Faradaic yield within 100 min, 72% conversion from 50 mM Et_3NHBF_4) are comparable to those of **LNi^{II}Fe^{II}Cp** (16 turnovers achieved, 70% conversion within 100 min and Faradaic yield of 70%). However, the mononuclear Fe^{II} precursor, $[Cp^*Fe^{II}(CO)(MeCN)_2]^+$, displays no reactivity toward protons under similar conditions; $[NiL^{N2S2}]$ produces H_2 but with a minor activity (9 turnovers achieved within 100 min).

DFT calculations (see DFT Mechanistic Investigations) proposed an CEEC mechanism starting from the reduced **LNi^{I}Fe^{II}Cp*** species that is consistent with this electrochemical set of data. Foot of the wave analysis (FOWA) has been realized in order to gain kinetics-related information for the H_2 production catalytic cycle.[43,44] A scan rate and acid concentration independent second-order rate constant (k_{cat}) of (6.8 ± 0.3) × 10^3 M^{-1} s^{-1} was determined.

DFT Mechanistic Investigations. To gain further insights into the mechanism of electrocatalytic H_2 production by **LNi^{II}Fe^{II}Cp***, DFT calculations have been performed and a full mechanism is proposed in Scheme 3 and Scheme S2 (at the B3P86 level). First, we focused on the rationalization of the redox properties of **LNi^{II}Fe^{II}Cp*** in the absence of protons. The DFT optimized structure of **LNi^{II}Fe^{II}Cp*** ($[\mathbf{1}^*]^+$; note that specific notations are used for the DFT optimized structures), with a singlet ground spin state, is fully consistent with the structural data obtained on **LNi^{II}Fe^{II}Cp*** by X-ray diffraction (less than 0.02 Å errors; Figure S13 and Tables S3 and S4). In addition, DFT calculations reproduce the IR frequencies of CO vibration for the Cp* and Cp complexes, as well as the large difference in their redox potentials E° (see Tables S5 and S6). The first reduction process is predicted to occur at E_{cal} = −1.19 V (−1.44 V at the TPSS level), in agreement with the CV that displays a first irreversible redox

DOI: 10.1021/acscatal.8b02830
ACS Catal. 2018, 8, 10658−10667

Scheme 3. DFT(B3P86) Calculated H_2 Production Catalytic Cycle for $LNi^{II}Fe^{II}Cp^*$[a]

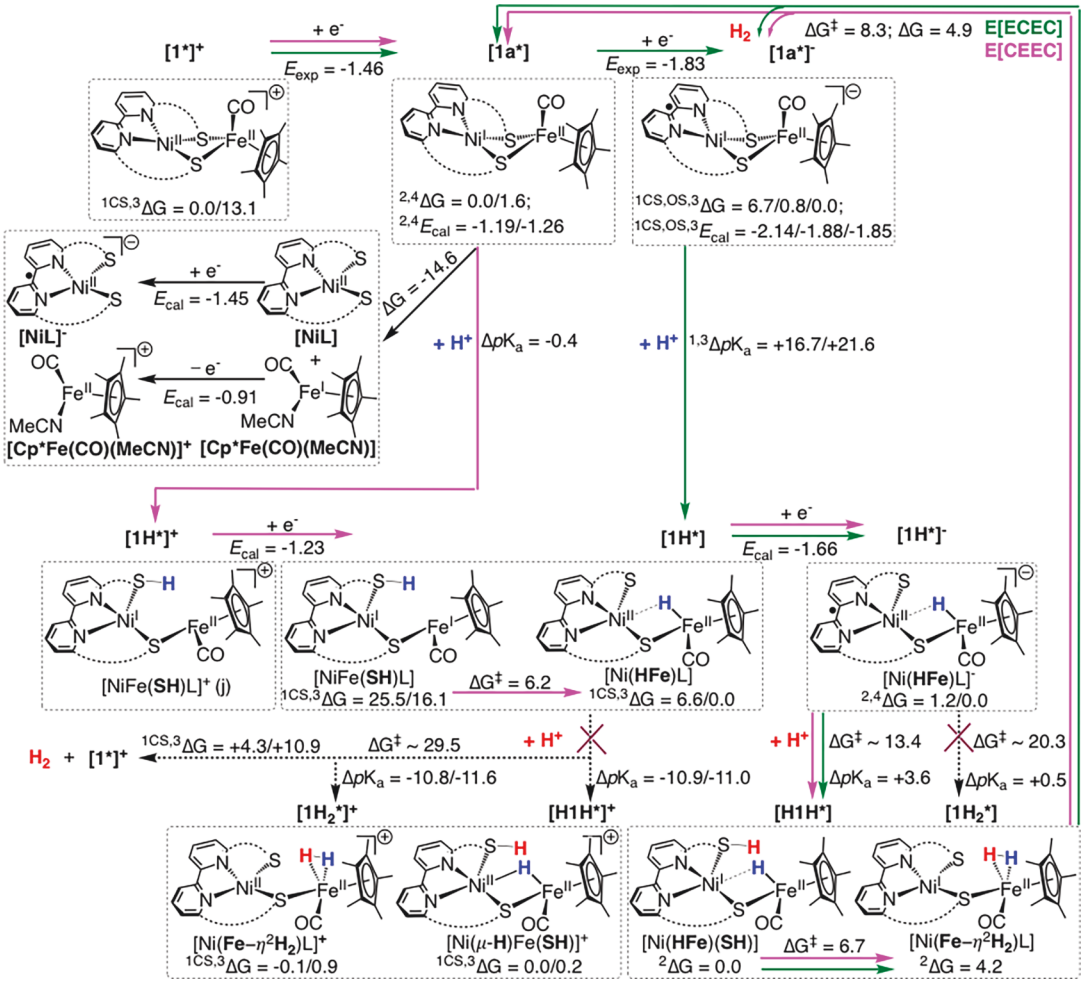

[a]The relative Gibbs free energies (ΔG) and barriers ($\Delta G^{\ddagger}$) are given in kcal/mol. The reduction potentials (E° vs $Fc^{+/0}$) are given in V. CS and OS indicate the closed-shell singlet and open-shell singlet states, respectively. The superscript numbers indicate the spin state. The relative acidities (ΔpK_a = pK_a(CatH) − pK_a(Et_3NH^+)) are reported with reference to Et_3NH^+ in MeCN. The more positive ΔpK_a values indicate that the protonation reaction is thermodynamically favorable, while the more negative ΔpK_a values indicate that the protonation reaction is thermodynamically unfavorable. The green arrow indicates the E[ECEC] pathway, while the pink arrow indicates the E[CEEC] pathway. All of the optimized geometries and the other tests are displayed in the Supporting Information.

system at E_{pc} = −1.46 V (Scheme 3). This one-electron-reduction process is Ni-based and generates the Ni^IFe^{II} species [**1a***] (spin density of 0.68 for the Ni ion and −0.01 for the Fe ion; Figure S14), as with the Cp derivative. However, in [**1a***], the CO molecule is terminally bound to the Fe unit instead of bridging between the metallic ions in the Cp derivative. This difference is proposed to be at the origin of the instability of **$LNi^{II}Fe^{II}Cp^*$**, resulting in the evolution to form [NiL^{N2S2}] and a FeCp*-based species. We investigated this decomposition process by computing the reduction potentials of all possible units, including $[FeCp^*(CO)]^{0/+}$ (E_{calc} = −0.47 V), $[FeCp^*(CO)(MeCN)]^{0/+}$ (E_{calc} = −0.91 V), and $[FeCp^*(CO)(MeCN)_2]^{0/+}$ (E_{calc} = −1.36 V) (Table S11). In agreement with the experimental data (E_{pa} = −1.04 V), it can be concluded that the generated [**1a***] species decomposes into [NiL^{N2S2}] and [$FeCp^*(CO)(MeCN)$]. Consistently, this process is calculated to be thermodynamically favorable (ΔG = −14.6 kcal mol^{-1}). The second reduction process is predicted to occur at E_{calc} = −1.85 V, in agreement with the experimental data ($E_{1/2}$ = −1.83 V), leading to the formation of $[\mathbf{1a}^*]^-$ through a ligand-based reduction. The spin density indicates that the bipyridine moiety acts as an electron reservoir and that the Ni ion remains in the +I oxidation state (Figure S15). Therefore, the experimentally observed redox system is proposed from the DFT calculations to originate from the reductions of [NiL^{N2S2}] combined with the potential contribution of [**1a***].

In the presence of $[Et_3NH]^+$, a catalytic wave develops on top of the second wave in the CV of **$LNi^{II}Fe^{II}Cp^*$**. DFT calculations at the B3P86 level predict that protonation of the one-electron-reduced [**1a***] species is thermodynamically feasible on the basis of the ΔpK_a value found for the most stable isomer among the 10 calculated isomers of $[\mathbf{1H}^*]^+$ (Scheme S4). Although the B3P86 ΔpK_a (vs $[Et_3NH]^+$) value of −0.4 is slightly unfavorable, positive ΔpK_a values are found with other functionals (+6.3 for B3LYP). Thus, the direct protonation of [**1a***] to $[\mathbf{1H}^*]^+$ is likely and is consistent with experimental data. The most stable isomer of $[\mathbf{1H}^*]^+$ corresponds to the protonation of one bridging thiolate, leading to its partial decoordination, and to the generation of a terminal-thiol-based Ni^I species (Scheme 3). $[\mathbf{1H}^*]^+$ is then

DOI: 10.1021/acscatal.8b02830
ACS Catal. 2018, 8, 10658−10667

reduced into [**1H***] at a predicted potential, which is very close to that for the first reduction.

At the experimental value for catalytic H_2 production ($E_{1/2}$ = −1.83 V), the calculations predict that, if [**1a***] is not directly protonated, it is reduced to [**1a***]$^-$, which is followed by a favorable protonation step (ΔpK_a (vs [Et_3NH]$^+$) = +21.6) to give [**1H***] (Scheme 3). The structure of the most stable isomers of [**1H***] (among seven calculated isomers, Scheme S5) corresponds to a hydride $Ni^{II}Fe^{II}$ species, in which one thiolate is no longer coordinated to the iron (Figure S17a). Decoordination of one bridging thiolate from a $Ni^{II}(\mu\text{-SR})_2Fe^{II}$ complex during electrocatalytic H_2 evolution has been also proposed by Hall, Darensbourg, and co-workers in a recent work[31] and by Tang and Hall for **LNi^{II}(H)Fe^{II}Cp**.[29] The hydride is bridging between the two metallic ions in [**1H***] with a shorter Fe−H bond of 1.55 Å (vs Ni−H, 1.75 Å; Figure S17a). The terminal Ni hydride and Fe hydride species have higher free energy than the semibridging NiFe hydride species (29.9 and 10.2 kcal mol^{-1}, respectively).

Neither the terminal thiolate nor the hydride in the singlet or triplet [**1H***] is basic enough to be protonated to form the thiol hydride [**H1H***]$^+$ or the side-on Fe η^2-H_2 complex [**1H$_2$***]$^+$, as indicated by the negative ΔpK_a values (vs [Et_3NH]$^+$) of −10.9/−11.0 and −10.8/−11.6, respectively. In addition, direct proton delivery from [Et_3NH]$^+$ to the hydride in [**1H***] to produce H_2 can be ruled out, since this process is both thermodynamically ($^{1CS,3}\Delta G$ = 4.3/10.9 kcal mol^{-1}) and kinetically ($\Delta G^{\ddagger} \approx$ 29.5 kcal mol^{-1}) unfavorable. Thus, a third one-electron-reduction process must occur prior to a second protonation step.

The reduction of [**1H***] to [**1H***]$^-$ is predicted to occur at the bipyridine ligand (Figure S18), with a calculated reduction potential for this couple at E_{cal} = −1.66 V. As this potential is less negative than that of the [**1a***]$^{-/0}$ couple by 0.19 V (Scheme 3), this process is consistent with electrocatalytic data.

Upon addition of the second proton to [**1H***]$^-$, two protonation sites can be envisaged: (i) the terminal thiolate, leading to the thiol hydride complex [**H1H***], or (ii) the bridging hydride, to generate the side-on Fe η^2-H_2 complex [**1H$_2$***]. On the basis of DFT calculations, the formation of [**H1H***] is predicted to be kinetically ($\Delta(\Delta G^{\ddagger})$ = 6.9 kcal mol^{-1}) and thermodynamically ($\Delta(\Delta G)$ = 0.4 kcal mol^{-1}) more favorable than that of [**1H$_2$***] (Scheme 4). On the basis of these considerations, after the protonation of [**1H***]$^-$ to form [**H1H***] (ΔpK_a = +3.6), the proton and the hydride react together ($\Delta G^{\ddagger}$ = 6.7 kcal mol^{-1}) to yield [**1H$_2$***]. Finally, H_2 is released from [**1H$_2$***] with the concomitant regeneration of the reduced species [**1a***] ($\Delta G^{\ddagger}$ = 8.3 kcal mol^{-1} and ΔG = 4.9 kcal mol^{-1}). Interestingly, in [**H1H***]$^+$, the hydride is symmetrically bridging both metallic ions (Fe−H and Ni−H distances of 1.63 and 1.62 Å, respectively) and is oriented toward the proton of the thiol in such a way that the H···H distance is about 2.9 Å (Figure S19). Such an arrangement is also found in the *Ni-R* state of the enzyme, in which the hydride species is also bridging but is shifted toward the Ni site (Fe−H and Ni−H distances of 1.72 and 1.57 Å, respectively) and is located at 2.45 Å away from the proton of a thiol terminally bound to the Ni site.[14] A similar intermediate has been also proposed in the case of a $Ni^{II}(\mu\text{-SR})_2Fe^{II}$ electrocatalyst, for which DFT calculations predict a thiol-containing Fe-based hydride intermediate, but the hydride is terminally bound to the iron ion.[31] Such an intermediate is also found in the catalytic cycle of [FeFe]-hydrogenase and its synthetic models, for which a terminal Fe-bound hydride and an ammonium are generated as the last intermediates prior to the formation of H_2 (or the first intermediate arising from the heterolytic cleavage of H_2).[45−47] In a broader context, **LNi^{II}Fe^{II}Cp*** thus represents an additional model of a H_2-evolving electrocatalyst in which the H−H bond is formed through the reaction between a pendant acid and a metal hydride, confirming the importance of such a structural motif.[48−51]

On the basis of the DFT-predicted mechanism, after a first reduction step required to activate **LNi^{II}Fe^{II}Cp*** and generate a $Ni^{I}Fe^{II}$ species, the catalytic H_2 evolution cycle is proposed to follow either an ECEC or an CEEC mechanism (Scheme 3). However, since it has been experimentally observed that **LNi^{I}Fe^{II}Cp*** interacts with [Et_3NH]$^+$, the E[CEEC] mechanism can be proposed as the main pathway. As in the [NiFe]-hydrogenase, especially in the *Ni-R* and *Ni-L* states,[5,14] protonation of a terminal Ni-bound thiolate is predicted to occur in the presence of a relatively weak acid (in [**H1H***]). So far only one structural and functional NiFe model has been shown to undergo protonation of a terminal Ni-bound thiolate, but this occurs only under strongly acidic conditions, irrelevant to those used in the catalytic assay.[52]

A recent work described by Darensbourg and Hall highlighted the hemilability of bridging thiolates in such types of catalysts during protonation steps. In their systems the redox chemistry mainly occurred on the Fe site and the hydride species were predicted to be terminally bound to the Fe ion.[31] It is worth noting that, in the mechanism proposed for both **LNi^{II}Fe^{II}Cp** and **LNi^{II}Fe^{II}Cp*** electrocatalysts, the redox chemistry occurs on the Ni site (including the bound bipyridine unit) and the protonation steps occur on both a terminal thiolate and the metallic sites through formation of a bridging hydride. Such a reactivity is similar to that observed for the [NiFe]-hydrogenase, even if in both the *Ni-R* and *Ni-C* states the hydride ligand is shifted toward the Ni site.[14]

Effect of CO Addition on Electrocatalytic Proton Reduction. The CVs of **LNi^{II}Fe^{II}Cp** and **LNi^{II}Fe^{II}Cp*** recorded in the presence of CO demonstrate that their redox properties are modified by CO addition. When CO is bubbled into a solution of **LNi^{II}Fe^{II}Cp***, the first cathodic peak is shifted from −1.46 to −1.41 V vs Fc^+/Fc and the corresponding backward peak at E_{pa} = −1.04 V is suppressed (Figure 3). This supports an interaction of CO with **LNi^{I}Fe^{II}Cp*** and its further stabilization (no more decomposition at the CV time scale is observed). CO binding

Scheme 4. Two DFT(B3P86) Calculated Pathways for the Protonation of [1H*]$^-$ (TEA = Et_3N)

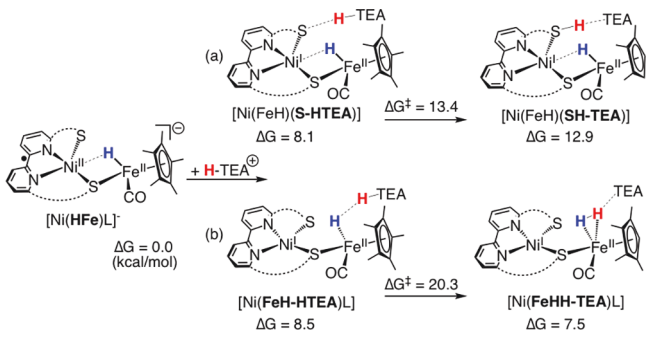

DOI: 10.1021/acscatal.8b02830
ACS Catal. 2018, 8, 10658−10667

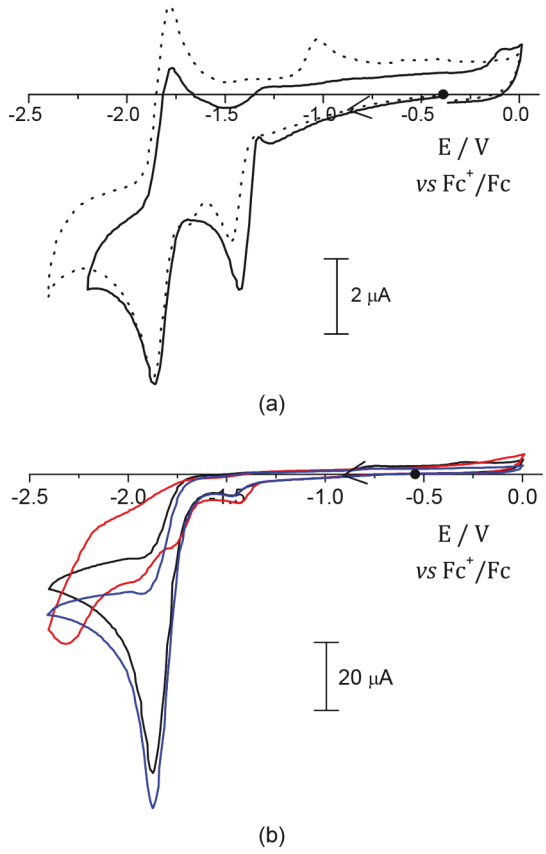

Figure 3. (a) CVs of $\mathbf{LNi^{II}Fe^{II}Cp^{*}}$ before (dotted line) and after (solid line) CO bubbling (0.2 mM solution in MeCN/0.1 M *n*-Bu_4NClO_4, glassy-carbon electrode, 100 mV s^{-1}). (b) CVs of $\mathbf{L^{N2S2}Ni^{II}Fe^{II}Cp^{*}}$ (same conditions as in (a)) in the presence of 15 equiv of $[Et_3NH]^+$ before (black line) and after (red line) CO bubbling and after successive Ar bubbling (blue line).

stabilizes the dinuclear Ni^IFe^{II} complex because of the strong π-acceptor character of CO that decreases the electronic density on the Ni^I ion.

The case of $\mathbf{LNi^{II}Fe^{II}Cp}$ is different (Figure S7): while the first reduction system remains almost unchanged after bubbling CO, a partial loss of the reversibility of the second reduction signal is observed, accompanied by an anodic shift ($E_{1/2}$ is displaced from −1.91 to −1.87 V). The fact that only the second redox reduction system of $\mathbf{LNi^{II}Fe^{II}Cp}$ is affected by the presence of CO evidences that CO exclusively interacts with its two-electron-reduced form, $\mathbf{L^{\bullet}Ni^{I}Fe^{II}Cp}$.[26]

The H_2 evolution activity of both electrocatalysts was also assessed in the presence of CO by cyclic voltammetry. When CO is bubbled into a MeCN solution containing 15 equiv of $[Et_3NH]^+$, the electrocatalytic activity of $\mathbf{LNi^{II}Fe^{II}Cp}$ is partially inhibited (about 30% loss, Figure S7), while for $\mathbf{LNi^{II}Fe^{II}Cp^{*}}$ a quasi-complete inhibition occurs (about 90% loss) (Figure 3). As expected, when CO is removed from the solution by argon bubbling, the activity of both complexes is restored.

DFT calculations gave insights into the inhibition of the H_2 evolution activity by CO. The structures of the CO adducts in both the Cp and Cp* systems were computed. For simplicity, Scheme 5 shows only the most stable CO adducts, while the other optimized species are displayed in Scheme S6. The calculations predict that all of the cationic ($[\mathbf{1a^{*}}]^+$ and $[\mathbf{1a}]^+$), neutral ($[\mathbf{1a^{*}}]$ and $[\mathbf{1a}]$), and anionic species ($[\mathbf{1a^{*}}]^-$ and $[\mathbf{1a}]^-$) are able to react with CO but to different degrees. The most stable adduct species are found to have one broken Fe−S bond. CO is terminally bound to the Fe ion for the cationic and neutral species, while it is (semi)bridging both metals for the anionic species (Figures S23 and S24).

In the presence of CO and in the absence of protons, the CV of $\mathbf{LNi^{II}Fe^{II}Cp^{*}}$ evidences an effect on the first reduction process, while for $\mathbf{LNi^{II}Fe^{II}Cp}$ the influence of CO is observed only on the second reduction process. This is consistent with the computational results (Scheme 5). First, the interaction of CO with the one-electron-reduced species $[\mathbf{1a^{*}}]$ is thermodynamically more favorable (ΔG = −17.2 kcal mol^{-1}) than with $[\mathbf{1a}]$ (ΔG = −1.3 kcal mol^{-1}). Second, binding of CO with the two-electron-reduced species $[\mathbf{1a}]^-$ is thermodynamically more favorable (ΔG = −6.1 kcal mol^{-1}) than with $[\mathbf{1a}]$.

Furthermore, the affinity of CO for $[\mathbf{1a^{*}}]^-$ is largely thermodynamically favorable, leading to a $L^{\bullet}Ni^{I}Fe^{II}$ species in which CO is bridging between the two metallic ions (Fe−CO and Ni−CO distances of 1.89 and 2.03 Å, respectively; Figure S23). A similar structure is observed in the interaction of CO with $[\mathbf{1a}]^-$ (Figure S24).

These calculations can fully rationalize the observed electrocatalytic activity of both $\mathbf{LNi^{II}Fe^{II}Cp}$ and $\mathbf{LNi^{II}Fe^{II}Cp^{*}}$ complexes in the presence of CO and protons: a partial inhibition for H_2 production with $\mathbf{LNi^{II}Fe^{II}Cp}$ (about 30% loss) vs a quasi-complete inhibition with $\mathbf{LNi^{II}Fe^{II}Cp^{*}}$ (about 90% loss). Indeed, the interactions of both one- and two-electron-reduced species for the Cp* derivatives $[\mathbf{1a^{*}}]$ and $[\mathbf{1a^{*}}]^-$ with CO are calculated to be thermodynamically more favorable than those of Cp derivatives $[\mathbf{1a}]$ and $[\mathbf{1a}]^-$.

CONCLUSION

This study highlights how ligand design can be used to finely tune the reactivity of bioinspired [NiFe]-hydrogenase complexes. Substituting the pentamethylcyclopentadienyl (Cp^{*-}) for the cyclopentadienyl (Cp^-) ligand at the Fe center in $\mathbf{LNi^{II}Fe^{II}Cp^{(*)}}$ complexes leads to remarkable modifications in terms of structural properties, especially for the $\{Ni(\mu\text{-}S)_2Fe\}$ core with a quasi-diamond structure in $\mathbf{LNi^{II}Fe^{II}Cp^{*}}$ in comparison to a butterfly structure in $\mathbf{LNi^{II}Fe^{II}Cp}$. Even when both complexes evolve H_2 with similar mechanisms, the structures of the catalytically active Ni^IFe^{II} species display a notable difference, with the CO ligand bridging both metals in the Cp derivative and being terminally bound to the Fe ion in the Cp* species. These differences translate into a more pronounced instability of the one-electron-reduced form of the Cp* derivative, $\mathbf{LNi^{I}Fe^{II}Cp^{*}}$. However, the dinuclear structure of this reduced species is retained under catalytically relevant conditions and $\mathbf{LNi^{II}Fe^{II}Cp^{*}}$ proves to be only slightly slower than $\mathbf{LNi^{II}Fe^{II}Cp}$ in catalyzing H_2 evolution. The most important difference between these two complexes is in the electrocatalytic H^+ reduction activity in the presence of CO: only partial inhibition (about 30% loss) is observed with $\mathbf{LNi^{II}Fe^{II}Cp}$, while the inhibition is quasi-complete (about 90% loss) with $\mathbf{LNi^{II}Fe^{II}Cp^{*}}$. In addition, the electrochemical behavior of $\mathbf{LNi^{II}Fe^{II}Cp^{*}}$ in the presence of CO combined with the DFT investigation evidenced that CO can bind to $\mathbf{LNi^{I}Fe^{II}Cp^{*}}$, a model of the *Ni-L* state. Since it is currently proposed that CO inhibition of [NiFe]-hydrogenase occurs only through the *Ni-SCO* state (Ni^{II}−CO), this work suggests that *Ni-CO* (Ni^{I}−CO), formed from *Ni-L*, may also be involved in this inhibition process.

DOI: 10.1021/acscatal.8b02830
ACS Catal. 2018, 8, 10658−10667

Scheme 5. Thermodynamic Data (kcal mol^{-1}) for the Interaction of CO with Cationic, Neutral, and Anionic Species in both Cp* and Cp Derivatives

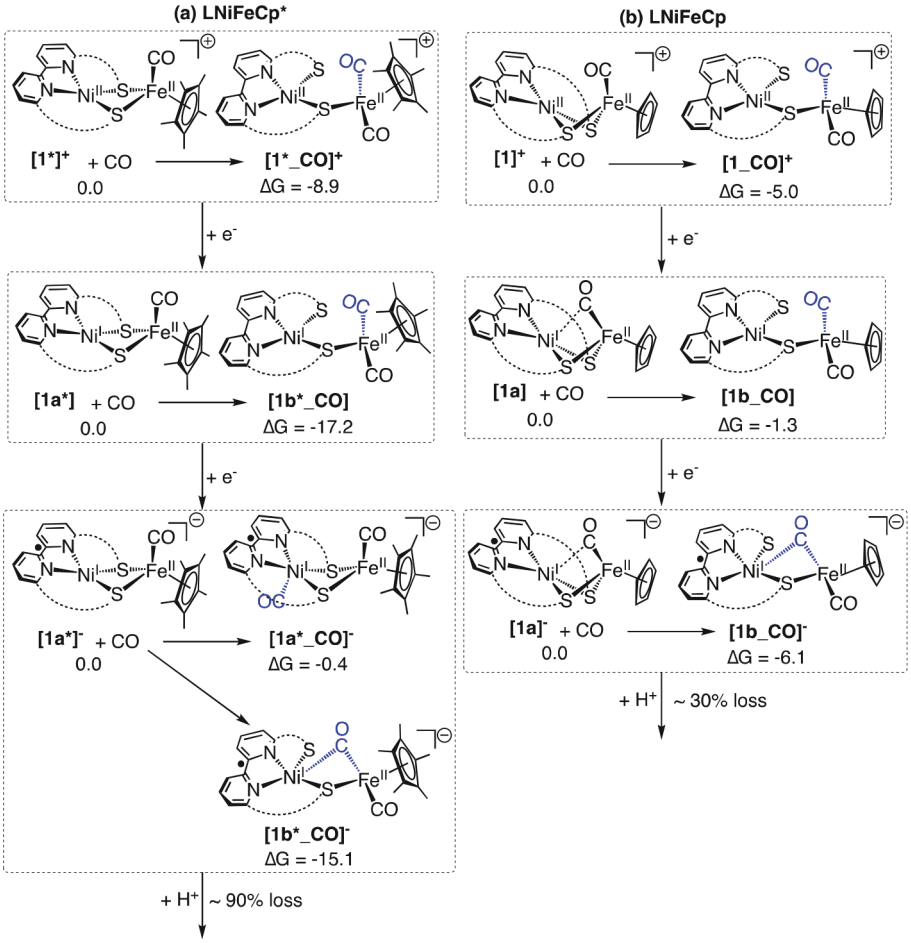

■ ASSOCIATED CONTENT

Supporting Information

The Supporting Information is available free of charge on the ACS Publications website at DOI: 10.1021/acscatal.8b02830.

Crystallographic data for **LNi^{II}Fe^{II}Cp*** (CIF)

Experimental section, characterization data (X-ray crystallography, ^{1}H NMR, Mössbauer, ESI-MS, CV, H_2 production, etc.), estimation of kinetic/catalytic parameters by electrochemical data, and computational details (PDF)

Cartesian coordinates for the calculated structures (PDF)

■ AUTHOR INFORMATION

Corresponding Authors

*E-mail for V.A.: vincent.artero@cea.fr.
*E-mail for M.B.H.: hall@science.tamu.edu.
*E-mail for C.D.: carole.duboc@univ-grenoble-alpes.fr.

ORCID

Marcello Gennari: 0000-0001-5205-1123
Franc Meyer: 0000-0002-8613-7862
Maylis Orio: 0000-0002-9317-8005
Carole Duboc: 0000-0002-9415-198X

Author Contributions

#D.B., L.W., and H.T. contributed equally to this work.

Notes

The authors declare no competing financial interest.

■ ACKNOWLEDGMENTS

Financial support for this work was provided by Labex arcane (ANR-11-LABX-003), the Agence National de la Recherche, the Deutsche Forschungsgemeinschaft (Grant Nos. ANR-16-CE92-0012-01 and DFG Me1313/14-1, NiFeMim), the Indo-French Center for the Promotion of Advanced Research (IFCPAR/CEFIPRA Grant No. 5405-1), the COST Action CM1305 (EcostBio) including an STSM grant (COST-STSM-CM1305-26539) to D.B., and the China Scholarship Council (L.W.). The computational work was supported by the National Science Foundation (CHE-1664866) and the Welch Foundation (A-0648) to M.B.H. Computer time was provided by the TAMU High Performance Research Computing Facility. We also acknowledge Allyssa Ann Massie for her help in IR spectroelectrochemistry.

■ REFERENCES

(1) Lubitz, W.; Ogata, H.; Rüdiger, O.; Reijerse, E. *Chem. Rev.* **2014**, *114*, 4081−4148.
(2) Frey, M. Hydrogenases: Hydrogen-Activating Enzymes. *ChemBioChem* **2002**, *3*, 153−160.
(3) Volbeda, A.; Charon, M.-H.; Piras, C.; Hatchikian, E. C.; Frey, M.; Fontecilla-Camps, J. C. Crystal structure of the nickel-iron hydrogenase from Desulfovibrio gigas. *Nature* **1995**, *373*, 580−587.

DOI: 10.1021/acscatal.8b02830
ACS Catal. 2018, 8, 10658−10667

(4) Ash, P. A.; Hidalgo, R.; Vincent, K. A. Proton Transfer in the Catalytic Cycle of [NiFe] Hydrogenases: Insight from Vibrational Spectroscopy. *ACS Catal.* **2017**, *7*, 2471−2485.
(5) Ogata, H.; Lubitz, W.; Higuchi, Y. Structure and function of [NiFe] hydrogenases. *J. Biochem.* **2016**, *160*, 251−258.
(6) Tai, H.; Higuchi, Y.; Hirota, S. Comprehensive reaction mechanisms at and near the Ni-Fe active sites of [NiFe] hydrogenases. *Dalton Trans.* **2018**, *47*, 4408−4423.
(7) van der Zwaan, J. W.; Albracht, S. P. J.; Fontijn, R. D.; Slater, E. C. Monovalent nickel in hydrogenase from Chromatium vinosum: Light sensitivity and evidence for direct interaction with hydrogen. *FEBS Lett.* **1985**, *179*, 271−277.
(8) Niu, S.; Thomson, L. M.; Hall, M. B. Theoretical Characterization of the Reaction Intermediates in a Model of the Nickel−Iron Hydrogenase of Desulfovibrio gigas. *J. Am. Chem. Soc.* **1999**, *121*, 4000−4007.
(9) Murphy, B. J.; Hidalgo, R.; Roessler, M. M.; Evans, R. M.; Ash, P. A.; Myers, W. K.; Vincent, K. A.; Armstrong, F. A. Discovery of Dark pH-Dependent H+ Migration in a [NiFe]-Hydrogenase and Its Mechanistic Relevance: Mobilizing the Hydrido Ligand of the Ni-C Intermediate. *J. Am. Chem. Soc.* **2015**, *137*, 8484−8489.
(10) Hidalgo, R.; Ash, P. A.; Healy, A. J.; Vincent, K. A. Infrared Spectroscopy During Electrocatalytic Turnover Reveals the Ni-L Active Site State During H_2 Oxidation by a NiFe Hydrogenase. *Angew. Chem., Int. Ed.* **2015**, *54*, 7110−7113.
(11) Brecht, M.; van Gastel, M.; Buhrke, T.; Friedrich, B.; Lubitz, W. Direct Detection of a Hydrogen Ligand in the [NiFe] Center of the Regulatory H_2-Sensing Hydrogenase from Ralstonia eutropha in Its Reduced State by HYSCORE and ENDOR Spectroscopy. *J. Am. Chem. Soc.* **2003**, *125*, 13075−13083.
(12) Foerster, S.; Stein, M.; Brecht, M.; Ogata, H.; Higuchi, Y.; Lubitz, W. Single Crystal EPR Studies of the Reduced Active Site of [NiFe] Hydrogenase from Desulfovibrio vulgaris Miyazaki F. *J. Am. Chem. Soc.* **2003**, *125*, 83−93.
(13) George, S. J.; Kurkin, S.; Thorneley, R. N. F.; Albracht, S. P. J. Reactions of H2, CO, and O2 with Active [NiFe]-Hydrogenase from Allochromatium vinosum. A Stopped-Flow Infrared Study. *Biochemistry* **2004**, *43*, 6808−6819.
(14) Ogata, H.; Nishikawa, K.; Lubitz, W. Hydrogens detected by subatomic resolution protein crystallography in a [NiFehydrogenase. *Nature* **2015**, *520*, 571−574.
(15) van der Zwaan, J. W.; Albracht, S. P. J.; Fontijn, R. D.; Roelofs, Y. B. M. EPR evidence for direct interaction of carbon monoxide with nickel in hydrogenase from Chromatium vinosum. *Biochim. Biophys. Acta, Protein Struct. Mol. Enzymol.* **1986**, *872*, 208−215.
(16) Fauque, G. U. Y.; Berlier, Y.; Choi, E. S.; Peck, H. D.; Le Gall, J.; Lespinat, P. A. The carbon monoxide inhibition of the proton-deuterium exchange activity of iron, nickel-iron and nickel-iron-selenium hydrogenases from Desulfovibrio vulgaris Hildenborough. *Biochem. Soc. Trans.* **1987**, *15*, 1050.
(17) Happe, R. P.; Roseboom, W.; Albracht, S. P. J. Pre-steady-state kinetics of the reactions of [NiFe]-hydrogenase from Chromatium vinosum with H2 and CO. *Eur. J. Biochem.* **1999**, *259*, 602−608.
(18) Ogata, H.; Mizoguchi, Y.; Mizuno, N.; Miki, K.; Adachi, S.-I.; Yasuoka, N.; Yagi, T.; Yamauchi, O.; Hirota, S.; Higuchi, Y. Structural Studies of the Carbon Monoxide Complex of [NiFe]hydrogenase from Desulfovibrio vulgaris Miyazaki F: Suggestion for the Initial Activation Site for Dihydrogen. *J. Am. Chem. Soc.* **2002**, *124*, 11628−11635.
(19) Pandelia, M.-E.; Ogata, H.; Currell, L. J.; Flores, M.; Lubitz, W. Inhibition of the [NiFe] hydrogenase from Desulfovibrio vulgaris Miyazaki F by carbon monoxide: An FTIR and EPR spectroscopic study. *Biochim. Biophys. Acta, Bioenerg.* **2010**, *1797*, 304−313.
(20) Tard, C.; Pickett, C. J. Structural and Functional Analogues of the Active Sites of the [Fe]-, [NiFe]-, and [FeFe]-Hydrogenases. *Chem. Rev.* **2009**, *109*, 2245−2274.
(21) Ohki, Y.; Tatsumi, K. Thiolate-Bridged Iron−Nickel Models for the Active Site of [NiFe] Hydrogenase. *Eur. J. Inorg. Chem.* **2011**, *2011*, 973−985.
(22) Simmons, T. R.; Berggren, G.; Bacchi, M.; Fontecave, M.; Artero, V. Mimicking hydrogenases: From biomimetics to artificial enzymes. *Coord. Chem. Rev.* **2014**, *270*−*271*, 127−150.
(23) Kaur-Ghumaan, S.; Stein, M. [NiFe] hydrogenases: how close do structural and functional mimics approach the active site? *Dalton Trans.* **2014**, *43*, 9392−9405.
(24) Chambers, G. M.; Huynh, M. T.; Li, Y.; Hammes-Schiffer, S.; Rauchfuss, T. B.; Reijerse, E.; Lubitz, W. Models of the Ni-L and Ni-SIa States of the [NiFe]-Hydrogenase Active Site. *Inorg. Chem.* **2016**, *55*, 419−431.
(25) Perotto, C. U.; Marshall, G.; Jones, G. J.; Stephen Davies, E.; Lewis, W.; McMaster, J.; Schroder, M. A Ni(I)Fe(II) analogue of the Ni-L state of the active site of the [NiFe] hydrogenases. *Chem. Commun.* **2015**, *51*, 16988−16991.
(26) Brazzolotto, D.; Gennari, M.; Queyriaux, N.; Simmons, T. R.; Pécaut, J.; Demeshko, S.; Meyer, F.; Orio, M.; Artero, V.; Duboc, C. Nickel-centred proton reduction catalysis in a model of [NiFe] hydrogenase. *Nat. Chem.* **2016**, *8*, 1054−1060.
(27) Zhu, W.; Marr, A. C.; Wang, Q.; Neese, F.; Spencer, D. J. E.; Blake, A. J.; Cooke, P. A.; Wilson, C.; Schröder, M. Modulation of the electronic structure and the Ni−Fe distance in heterobimetallic models for the active site in [NiFe]hydrogenase. *Proc. Natl. Acad. Sci. U. S. A.* **2005**, *102*, 18280−18285.
(28) Canaguier, S.; Field, M.; Oudart, Y.; Pecaut, J.; Fontecave, M.; Artero, V. A structural and functional mimic of the active site of NiF[NiFe]-hydrogenases. *Chem. Commun.* **2010**, *46*, 5876−5878.
(29) Tang, H.; Hall, M. B. Biomimetics of NiFe -Hydrogenase: Nickel- or Iron-Centered Proton Reduction Catalysis? *J. Am. Chem. Soc.* **2017**, *139*, 18065−18070.
(30) Jeffrey, J. C.; Rauchfuss, T. B. Metal complexes of hemilabile ligands. Reactivity and structure of dichlorobis(o-(diphenylphosphino)anisole)ruthenium(II). *Inorg. Chem.* **1979**, *18*, 2658−2666.
(31) Ding, S.; Ghosh, P.; Lunsford, A. M.; Wang, N.; Bhuvanesh, N.; Hall, M. B.; Darensbourg, M. Y. Hemilabile Bridging Thiolates as Proton Shuttles in Bioinspired H2 Production Electrocatalysts. *J. Am. Chem. Soc.* **2016**, *138*, 12920−12927.
(32) Hsieh, C.-H.; Ding, S.; Erdem, Ö. F.; Crouthers, D. J.; Liu, T.; McCrory, C. C. L.; Lubitz, W.; Popescu, C. V.; Reibenspies, J. H.; Hall, M. B.; Darensbourg, M. Y. Redox active iron nitrosyl units in proton reduction electrocatalysis. *Nat. Commun.* **2014**, *5*, 3684.
(33) Ghosh, P.; Ding, S.; Chupik, R. B.; Quiroz, M.; Hsieh, C.-H.; Bhuvanesh, N.; Hall, M. B.; Darensbourg, M. Y. A matrix of heterobimetallic complexes for interrogation of hydrogen evolution reaction electrocatalysts. *Chem. Sci.* **2017**, *8*, 8291−8300.
(34) Ding, S.; Ghosh, P.; Darensbourg, M. Y.; Hall, M. B. Interplay of hemilability and redox activity in models of hydrogenase active sites. *Proc. Natl. Acad. Sci. U. S. A.* **2017**, *114*, E9775−E9782.
(35) Sun, P.; Yang, D.; Li, Y.; Zhang, Y.; Su, L.; Wang, B.; Qu, J. Thiolate-Bridged Nickel−Iron and Nickel−Ruthenium Complexes Relevant to the CO-Inhibited State of [NiFe]-Hydrogenase. *Organometallics* **2016**, *35*, 751−757.
(36) Ohki, Y.; Yasumura, K.; Ando, M.; Shimokata, S.; Tatsumi, K. A model for the CO-inhibited form of [NiFe] hydrogenase: synthesis of $(CO)_3Fe(\mu\text{-}S^tBu_3Ni\{SC_6H_3\text{-}2,6\text{-}(mesityl)_2\}$ and reversible CO addition at the Ni site. *Proc. Natl. Acad. Sci. U. S. A.* **2010**, *107*, 3994−3997.
(37) Matsumoto, T.; Kabe, R.; Nonaka, K.; Ando, T.; Yoon, K. S.; Nakai, H.; Ogo, S. Model Study of CO Inhibition of NiFe hydrogenase. *Inorg. Chem.* **2011**, *50*, 8902−8906.
(38) Pandelia, M.-E.; Ogata, H.; Lubitz, W. Intermediates in the Catalytic Cycle of [NiFe] Hydrogenase: Functional Spectroscopy of the Active Site. *ChemPhysChem* **2010**, *11*, 1127−1140.
(39) Canaguier, S.; Vaccaro, L.; Artero, V.; Ostermann, R.; Pecaut, J.; Field, M. J.; Fontecave, M. Cyclopentadienyl Ruthenium-Nickel Catalysts for Biomimetic Hydrogen Evolution: Electrocatalytic Properties and Mechanistic DFT Studies. *Chem. - Eur. J.* **2009**, *15*, 9350−9364.

DOI: 10.1021/acscatal.8b02830
ACS Catal. 2018, 8, 10658−10667

(40) Gennari, M.; Orio, M.; Pécaut, J.; Neese, F.; Collomb, M.-N.; Duboc, C. Reversible Apical Coordination of Imidazole between the Ni(III) and Ni(II) Oxidation States of a Dithiolate Complex: A Process Related to the Ni Superoxide Dismutase. *Inorg. Chem.* **2010**, *49*, 6399−6401.
(41) Izutsu, K. *Acid-Base Dissociation Constants in Dipolar Aprotic Solvents*. Blackwell Scientific: Oxford, U.K., 1990.
(42) Actually, the peak at E_{pa} = − 1.04 V is retained in the CV of $[Cp^*Fe^{II}(CO)(MeCN)_2]^+$ after addition of up to 15 equiv of Et_3NHBF_4 (Figure S6).
(43) Costentin, C.; Drouet, S.; Robert, M.; Savéant, J.-M. Turnover Numbers, Turnover Frequencies, and Overpotential in Molecular Catalysis of Electrochemical Reactions. Cyclic Voltammetry and Preparative-Scale Electrolysis. *J. Am. Chem. Soc.* **2012**, *134*, 11235−11242.
(44) Costentin, C.; Saveant, J.-M. Multielectron, Multistep Molecular Catalysis of Electrochemical Reactions: Benchmarking of Homogeneous Catalysts. *ChemElectroChem* **2014**, *1*, 1226−1236.
(45) Reijerse, E. J.; Pham, C. C.; Pelmenschikov, V.; Gilbert-Wilson, R.; Adamska-Venkatesh, A.; Siebel, J. F.; Gee, L. B.; Yoda, Y.; Tamasaku, K.; Lubitz, W.; Rauchfuss, T. B.; Cramer, S. P. Direct Observation of an Iron-Bound Terminal Hydride in FeFe -Hydrogenase by Nuclear Resonance Vibrational Spectroscopy. *J. Am. Chem. Soc.* **2017**, *139*, 4306−4309.
(46) Katz, S.; Noth, J.; Horch, M.; Shafaat, H. S.; Happe, T.; Hildebrandt, P.; Zebger, I. Vibrational spectroscopy reveals the initial steps of biological hydrogen evolution. *Chem. Sci.* **2016**, *7*, 6746−6752.
(47) Niu, S.; Hall, M. B. Modeling the Active Sites in Metalloenzymes 5. The Heterolytic Bond Cleavage of H_2 in the [NiFe] Hydrogenase of Desulfovibrio gigas by a Nucleophilic Addition Mechanism. *Inorg. Chem.* **2001**, *40*, 6201−6203.
(48) Bhattacharjee, A.; Andreiadis, E. S.; Chavarot-Kerlidou, M.; Fontecave, M.; Field, M. J.; Artero, V. A Computational Study of the Mechanism of Hydrogen Evolution by Cobalt(Diimine-Dioxime) Catalysts. *Chem. - Eur. J.* **2013**, *19*, 15166−15174.
(49) Rakowski DuBois, M.; DuBois, D. L. The roles of the first and second coordination spheres in the design of molecular catalysts for H2 production and oxidation. *Chem. Soc. Rev.* **2009**, *38*, 62−72.
(50) Rakowski Dubois, M.; Dubois, D. L. Development of Molecular Electrocatalysts for CO_2 Reduction and H_2 Production/Oxidation. *Acc. Chem. Res.* **2009**, *42*, 1974−1982.
(51) Fang, M.; Wiedner, E. S.; Dougherty, W. G.; Kassel, W. S.; Liu, T.; DuBois, D. L.; Bullock, R. M. Cobalt Complexes Containing Pendant Amines in the Second Coordination Sphere as Electrocatalysts for H2 Production. *Organometallics* **2014**, *33*, 5820−5833.
(52) Weber, K.; Krämer, T.; Shafaat, H. S.; Weyhermüller, T.; Bill, E.; van Gastel, M.; Neese, F.; Lubitz, W. A Functional [NiFe]-Hydrogenase Model Compound That Undergoes Biologically Relevant Reversible Thiolate Protonation. *J. Am. Chem. Soc.* **2012**, *134*, 20745−20755.

DOI: 10.1021/acscatal.8b02830
ACS Catal. 2018, 8, 10658−10667